Correction to the paper "A Random-Phase-Assisted Ray-Tracing Code for Wireless Channel Modeling" by authors Houtao Zhu, Jun-ichi Takada, Kiyomichi Araki, and Takehiko Kobayashi.

This paper appeared in Volume15, #3, (November 2000), a Special Issue of the ACES Journal, and starts on page126. The paper has two errors: figures 12 and 13 were incorrectly reproduced during the editing process. The paper has been reproduced in its entirety with correct figures and printed in this issue.

Please make a note of these two figures in your issue of the Journal.

Our apologies go to all the authors.

A random-phase-assisted ray-tracing code for wireless channel modeling

Houtao Zhu[1], Jun-ichi Takada[1], Kiyomichi Araki[2], and Takehiko Kobayashi[3]

[1]International Cooperation Center for Science and Technology,
[2]Department of Computer Engineering, Tokyo Institute of Technology 2-12-1 O-okayama, Meguro-ku, Tokyo 152-8550, JAPAN
[3]YRP Mobile Telecommunications Key Technology Research Laboratories Co., Ltd

Abstract— **A random-phase-assisted ray-tracing computer code for predicting spatio-temporal wireless channel parameters is presented. A two dimensional-three dimensional (2D-3D) hybrid ray-tracing algorithm is implemented in code for the prediction of channel parameters in outdoor micro- and pico-cellular urban environments. Meanwhile, a Random Phase Approach (RPA) is applied in the ray-tracing algorithm. The application of the RPA is intended for two-fold purposes: 1) to account for the effects of inaccurate antenna positions; 2) to predict the range of short-term fading fluctuation. Several measurements carried out in pico-cell environments confirm the calculation accuracy of the code. It was found that measured fluctuation of path-loss and delay profiles are almost fully confined within the 90% confidence interval, proving that the approach can account for the effects mentioned above. In addition, the conventional verification of path-loss and delay profiles predicted by ray tracing was extended to include the verification of angle-of-arrival (AOA). The demonstrated calculation accuracy in spatial and temporal domain confirms the applicability of authors' code to analyze system performance in real environments.**

I. Introduction

Recently, ray-tracing methods have become popular approaches applied in prediction of cell coverage in wireless networks [1]–[3] and even proposed for deterministic channel modeling [4]. In fact, an ray-tracing approach is a complex computer code which combines computer graphics techniques and numerical electromagnetic computation techniques (e.g., Uniform Theory of Diffraction (UTD)) together. Current ray-tracing methods mainly focus on predicting path loss or delay spread in the real environments [1]–[3][5]–[9]. However, the fast progress of spatio-temporal signal processing techniques (e.g., smart antenna) for next-generation wireless systems has demanded a complete accurate prediction of channel parameters not only temporally but also spatially for system performance evaluation. Nevertheless, the verification of predicting spatio-temporal channel parameters from ray tracing has not been fully completed. There is very few verification reported in the literature. In addition, a number of disadvantages inherent in existing ray-tracing methods frustrate people who use them. For example, although 3D ray-launching methods [1][5][7] launch rays from an icosahedron, they are launched with unequal separating angles that can deteriorate the accuracy of a calculation. Alternatively, image methods [3][6][8][9] normally require a substantial amount of memory to establish various order image sources. A worse disadvantage of ray tracing is that phases of rays can not be correctly predicted due to inaccurate coordinates of buildings and antenna positions. These phase errors can cause the totally wrong phase-summed result when the rays are summed in vector forms [1].

Therefore, the RPA [10][11] is applied in authors' code to address the phase-error problem by assuming the rays are with random phases. With this assumption, the statistical distribution of signal strength at each location (for path-loss prediction) and at each sampling instant (for delay-profile prediction) can be derived analytically. With this distribution, the phase-error problem can be mitigated by choosing a local mean value obtained from the distribution. Besides this effect, it was also found that the fluctuation range of fast-fading signal levels and delay profiles can be accurately predicted with the RPA. This range is impossible to be predicted with the conventional ray-tracing codes. In this paper, the RPA is incorporated with a 2D-3D hybrid ray-tracing method [12] to be proposed for predicting spatio-temporal channel parameters in outdoor micro- and pico-cellular environments.

The organization of this paper is as follows: Section 2 presents the detailed ray-tracing algorithm and the RPA. Section 3 describes the measurement and comparison of ray-tracing results with measurement data in: 1) path-loss, 2) delay profiles and 3) azimuth-delay profiles. Finally, section 4 draws conclusions on this ray-tracing code.

II. 2D-3D Hybrid Ray-Tracing Method

The purpose of the authors' ray-tracing code is to predict spatio-temporal channel parameters in micro- and pico-cellular environments. The following assumptions are made :

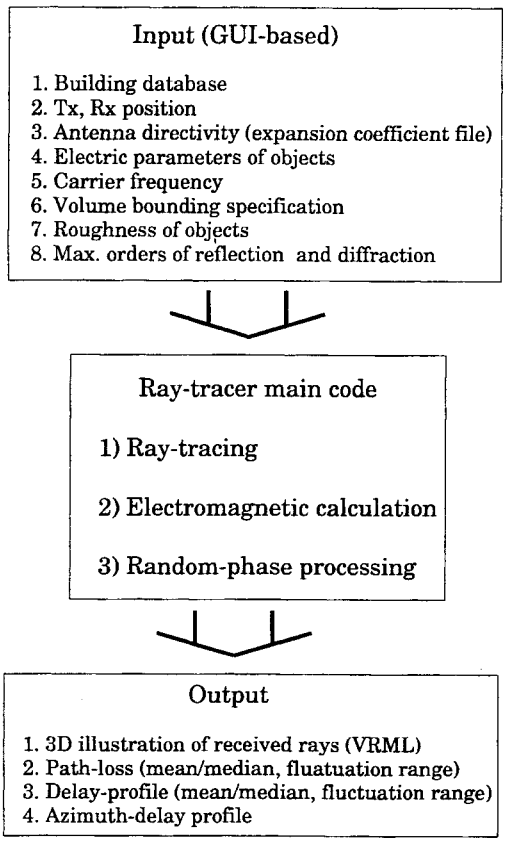

Fig. 1. Block diagram of the author's ray-tracing code

- Transmitting antenna heights are below the rooftops of surrounding buildings
- The ground is smooth and flat.
- Walls of buildings are perpendicular to the ground.

The main body of the authors' 2D-3D hybrid ray-tracing code can be divided into three parts: 1) Ray tracing, 2) Electromagnetic wave calculation, and 3) Random-phase processing (Fig. 1). Ray tracing traces rays from transmitter to receiver as efficiently as possible to find detailed ray paths. Electromagnetic wave calculation uses electromagnetic wave theory to calculate theoretical values in a realistic environment. The RPA is then applied to calculate the local mean or median value and a confidence interval which corresponds to the fluctuation range of fading.

A. Ray-Tracing Formulation

The 2D-3D hybrid ray-tracing method [12] is based on the ray-launching idea [5], which regards the transmitter as being a point source that launches rays in every direction. In the authors' approach, rays are launched in a 2-dimensional horizontal plane with equal angle separation. The location of the reflection and diffraction points and the formulation of reflected and diffracted rays are carried out based on Geometrical Optics (GO), Snell's Law of Reflection, and Keller's Law of Diffraction[13].

A.1 Determination of the ray path

When vertical walls are only considered, 2D tracing gives correct 3D results. The locations of reflection points are determined by simple line and line intersection in a 2-dimensional coordinate system. Since the incident angle should be equal to the reflection angle (the Law of Reflection), the reflected ray vector is determined by the following simple vector calculation [14]:

$$\hat{\boldsymbol{k}}_r = \hat{\boldsymbol{k}}_i - 2\,(\hat{\boldsymbol{n}} \cdot \hat{\boldsymbol{k}}_i)\,\hat{\boldsymbol{n}} \tag{1}$$

where

$\hat{\boldsymbol{k}}_i$: unit vector of the incident ray
$\hat{\boldsymbol{n}}$: unit vector of the surface normal
$\hat{\boldsymbol{k}}_r$: unit vector of the reflected ray

Building corners are checked by setting up capture circles to determine diffraction points [5]. As the incident angle (the angle between the incident ray and the edge of a building wall) is equal to the diffraction angle (the angle between the diffracted ray and the edge of a building wall), if we virtually unfold the incident plane and diffraction plane into one plane, the incident ray and the diffracted ray are actually in a straight line. After determining the intersection points, the ray paths are established by geometrically calculating the heights of intersection points. The height h_k of the kth reflection or diffraction point is obtained as:

$$h_k = \frac{L_{tk} \cdot h_r + h_t \cdot (L_{tr} - L_{tk})}{L_{tr}} \tag{2}$$

where

L_{tk} : 2D ray path length from the transmitter to the intersection point
L_{tr} : 2D ray path length from the transmitter to the receiver
h_t : the height of the transmitter
h_r : the height of the receiver

As each ray path generates a pair of rays (one with ground-reflection and one without), ground-reflected rays are formed by searching the ground-reflection point in the previous ray path. The ray path length from the transmitter to the ground-reflection point L_{tg} is calculated by:

$$L_{tg} = \frac{h_t \cdot L_{tr}}{h_t + h_r} \tag{3}$$

The ground-reflection point is formed along the ray path, and the heights of other intersection points are adjusted by the Eq. (3). Finally, the heights of intersection points are compared with the heights of the buildings. If one of the intersection points is higher than the building, the ray path does not exist.

The capture circle [5] is set up to determine whether the ray reaches each building corner and receiving point or not. The circle radius is defined as $0.5 \cdot \alpha \cdot L$, where α is the angle separation, and L is the whole length of the ray path between the source and the capture circle. Although calculation accuracy is improved when launching-angle separation is smaller, computational time increases. There is a tradeoff between accuracy and computational time with regard to launching-angle separation. In the authors' experiences, a 0.1° to 1° launching angle separation is sufficient for pico-cells (0.1°— 0.5° for $60 \times 60\ \mathrm{m}^2$) and micro-cells (0.5°— 1° for $600 \times 600\ \mathrm{m}^2$). In addition to the ray reaching the receiving point, ray tracing is terminated if one of the following three conditions is met:

1. The signal level of the ray is below the threshold value,
2. The intersection order of the ray exceeds the user-specified maximum reflection and diffraction number,
3. The ray leaves the whole area.

A.2 Application of ray-acceleration techniques

To decrease computational time, a series of ray-acceleration techniques [14] is used in the authors' ray-tracing code. These are:

1. Back-face Culling
   Since most of the computational time is spent on intersection checks, the authors' main intention is to reduce intersection-check times. The dot product of the normal vector of a surface (building wall) with the launching ray vector are used to determine if the wall is invisible to the launching ray (back-face). If the dot product is greater than zero, the building face is invisible to the launching ray and it does not need to be checked for an intersection.
2. Volume Bounding
   The volume bounding technique is used to reduce the number of buildings required for an intersection-check. An area is divided into several rectangular sub-areas (bounding volume) and users specify the size of the bounding volume. When the bounding volume intersected by the ray is determined, the buildings in that volume are checked for an intersection. Without this technique, every building in the area would have to be checked. Computational time would be then dramatically increased.
3. Partition Vector
   The authors propose Partition Vector (PV) as a simple but effective technique for ray-acceleration. The ray vector is bound with two partition vectors – unit vectors that start from the end point of the current ray vector and can be directed along positive/negative x or y-axis direction. A bounding area formed by using two partition vectors in one bounding volume is shown in Fig. 2. If the coordinates of one of the building's corners are confined in the bounding area, this building then qualifies for an intersection check.

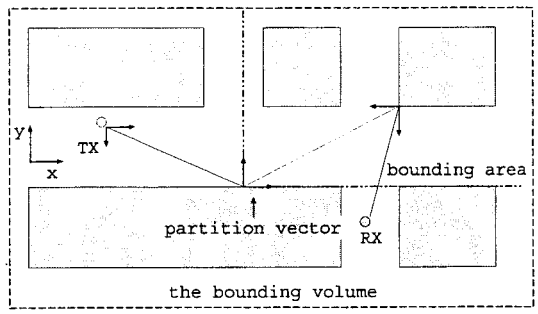

Fig. 2. Application of partition vectors in one bounding volume

B. Theoretical Calculation

The authors' ray-tracing code allows the user to specify the positions of the transmitter and the receiver, the electrical parameters (conductivity and permittivity) of every building and ground plane, and carrier frequency and the vector field directivity of antennas. Since in real environments building walls may not be smooth, the roughness of reflecting surfaces can be specified by the standard deviation of the surface height with respect to the mean surface height. The randomness of the surface height is assumed to be modeled by a Gaussian distribution.

B.1 Field calculation

The rotation of the polarization vector is considered for each reflection and diffraction event. The dyadic reflection and diffraction coefficients [15] are used for the field calculation. At reflection and diffraction points, the electric field components in the global coordinate system $E_{x,y,z}$ are first resolved into parallel and perpendicular components (with respect to the incidence plane) and multiplied by corresponding reflection/diffraction coefficients. After the calculation, the polarization components are resolved again to $E_{x,y,z}$ in the global Cartesian coordinate system. The average rough-surface reflection coefficient [16] and the heuristic dielectric wedge diffraction coefficient [17] from UTD are used for the calculation of reflection and diffraction loss.

The received electric field at the receiving antenna is therefore calculated by the following formulas:
Direct ray

$$\boldsymbol{E}_{\mathrm{LOS}} = \frac{\boldsymbol{E}_0}{d} e^{-jkd} \tag{4}$$

Reflected rays

$$\boldsymbol{E}_{\mathrm{R}} = \frac{\boldsymbol{E}_0}{d} \cdot \overline{\boldsymbol{R}}_{rough} e^{-jkd} \tag{5}$$

Once-diffracted rays

$$\boldsymbol{E}_{\mathrm{D}} = \frac{\boldsymbol{E}_0}{s'} \cdot \overline{\boldsymbol{R}}_{rough} \cdot \overline{\boldsymbol{D}} \sqrt{\frac{s'}{s(s'+s)}} e^{-jk(s+s')} \tag{6}$$

Twice-diffracted rays[1]

$$\boldsymbol{E}_{\mathrm{DD}} = \frac{\boldsymbol{E}_0}{s'} \cdot \overline{\boldsymbol{R}}_{rough} \cdot \overline{\boldsymbol{D}}_1 \cdot \overline{\boldsymbol{D}}_2 \sqrt{\frac{s'}{ss''(s'+s+s'')}} e^{-jk(s+s'+s'')} \tag{7}$$

where

$\boldsymbol{E}_0$: emitted electric field observed at the unit distance

d : propagation path length

s' : path length from the source to the first diffracting wedge

s : path length from the first diffracting wedge to the receiver (for once-diffracted rays) or to the second diffracting wedge (for twice-diffracted rays)

s'' : path length from the second diffracting wedge to the receiver

$\overline{\boldsymbol{R}}_{rough}$: dyadic reflection coefficient of the rough surface

$\overline{\boldsymbol{D}}$: dyadic diffraction coefficient of the dielectric wedge

The total field strength at any receiving point is contributed by reflected, diffracted and multiple reflected/-diffracted signals due to the multipath phenomena. This is calculated by the deterministic linear superposition of all single contributions as follows:

$$\boldsymbol{E}_{total} = \sum_{i=1}^{k} \boldsymbol{E}_i = \sum_{i=1}^{k} E_i \hat{\boldsymbol{e}} \cdot e^{j\phi_i} \tag{8}$$

where

$\hat{e}$: unit vector of polarization for i-th arrival ray

E_i : amplitude of i-th arrival ray ($|E_i|$)

ϕ_i : phase of i-th arrival ray

and ϕ_i is given as follows:

$$\phi_i = \psi_i - kd_i \tag{9}$$

where

ψ_i : phase shift caused by interaction with obstacles

d_i : propagation path length of i-th arrival ray

In the authors' approach, ϕ_i is assumed to be random. A statistical superposition of single contributions to calculate the total field strength is therefore adopted.

B.2 Calculation of the vector antenna pattern

Normally, the antenna radiation pattern used in ray tracing is approximated by the E and H plane patterns [18] or applied by a 3D radiation pattern stored in the computer [6]. The former may not be particularly accurate since the antenna emits rays in 3D. The latter wastes computer memory. In the authors' approach, far-field pattern functions $\boldsymbol{K}_{smn}(\theta,\phi)$ and the expansion coefficient Q_{smn} [19] express the field directivity pattern of the antenna. The index s distinguishes the two modes: $s = 1$ denotes TE mode and $s = 2$ denotes TM mode. The indices m and n indicate the mode numbers of the wave functions in the ϕ and θ directions respectively.

Since the radiating power of the antenna is given by:

$$P = \frac{1}{2} \sum\nolimits_{smn} |Q_{smn}|^2 \tag{10}$$

the transmitting power can be normalized to a 0 dB gain and the vector directivity function is obtained as:

$$\boldsymbol{D}(\theta,\phi) = \frac{\sum_{smn} Q_{smn} \boldsymbol{K}_{smn}(\theta,\phi)}{\sqrt{\sum_{smn} |Q_{smn}|^2}} \tag{11}$$

Therefore, if the field pattern of arbitrary antenna ($\boldsymbol{E}$) is given, the expansion coefficient is obtained by the following equation:

$$Q_{smn} = \oint_{\Omega} \boldsymbol{E} \cdot \boldsymbol{K}^*_{smn} d\Omega \tag{12}$$

The expansion coefficient is stored as a look-up table in the computer. Finally, the emitted field is calculated according to the Eq. (11) and resolved into $E_{x,y,z}$ components from spherical coordinates in the global coordinate system. The use of the far-field pattern function has some advantages. First, it strictly satisfies Maxwell's equations and is therefore widely used in spherical near-field antenna measurements [19]. Second, the mode number of the function, sufficient to the expansion, is limited and proportional to the antenna size. This can reduce the need for computer memory to store antenna patterns.

C. Random-Phase Processing

The conventional power-summing approach [20] sums up the power of each individual ray to obtain the total signal level by assuming that the incoming rays are incoherent. However, this approach can not indicate the fluctuation range of the signal level or demonstrate the fading phenomena. Alternatively, the phase-summing approach [20] calculates the total signal level from the sum of individual complex rays. Fast variation (multipath fading) of the signal can be observed in the total

signal level. However, the calculation is quite possibly corrupted by the phase errors of some rays. This approach also requires a sufficiently large averaging window to obtain the spatial average of the signal [20]. This large averaging window is not appropriate to micro- and pico-cell environments. In the authors' approach, the idea of random phase ray-tracing [10][11] is adopted to model the level of fluctuation due to the coherent interaction among different rays.

Since the building database and the positions of the antennas may not be accurate in the order of wavelength, a phase error is introduced into each ray. This may dramatically deteriorate the accuracy of the ray-tracing results. As the total field at the receiving point is expressed in Eq. (8), phase ϕ_i is therefore assumed to be random. The cumulative probability of the total field strength (fading statistics) at the receiving point can be derived by the characteristic function method and is given as [21]:

$$P(|E|) = \frac{2|E|}{R} \sum_{n=1}^{\infty} \frac{\Phi(\gamma_n/R)}{\gamma_n J_1^2(\gamma_n)} J_1\left(\frac{\gamma_n |E|}{R}\right) \tag{13}$$

where

γ_n : the n-th root of zeroth-order Bessel function $J_0(.)$

$J_1(.)$: the first order Bessel function.

and

$$\Phi(x) = \exp\left(-\frac{\sigma^2 x^2}{2}\right) \cdot \prod_{i=1}^{k} J_0(A_i x) \tag{14}$$

where

σ^2 : receiver noise power

A_i : the amplitude of the ith ray

and R is an upper limit parameter, as sufficiently large as possible and chosen as [22]:

$$R = \sum_{i=1}^{k} A_i + 5\sigma \tag{15}$$

The total field strength corresponding to the cumulative probability from 5% to 95% is selected as the confidence interval. The prediction error of ray-tracing approaches, caused by incorrect phases, can be improved by using the local mean calculated by the RPA. By incorporating the RPA into the ray-tracing method, it provides an insight into the fading mechanism and also a specific range, within which the signal level will fluctuate.

The RPA can be also applied to predict the fluctuation range of delay profiles [23]. The band-limited delay profiles are obtained by convolving the channel impulse response predicted from ray tracing with a channel filter. In fact, these delay profiles are sampled and the sampling interval is decided by the system bandwidth. At each sampling instant, the interaction between different impulses is occurred due to convolution, which can be represented as:

$$h(nT_s) = \sum_{i=1}^{n} A_i e^{j\phi_i} P(\tau_i - nTs) \tag{16}$$

where

T_s : symbol duration or chip duration

$P(t)$: impulse response of channel filter

Correspondingly, the RPA can be applied here by assuming ϕ_i is random.

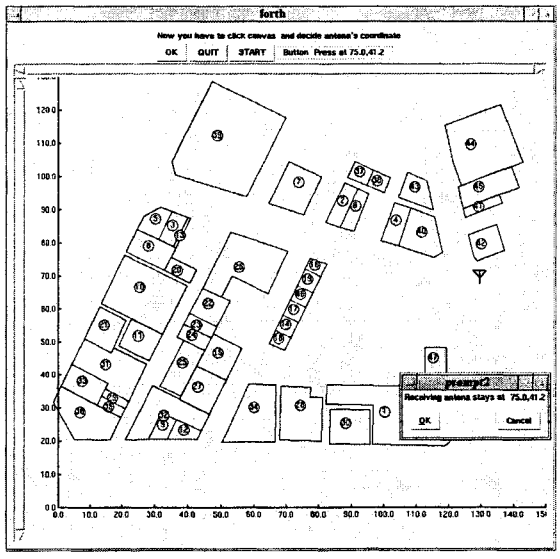

Fig. 3. GUI interface of the ray-tracing code

III. Field Measurement and Comparison Results

This ray-tracing code is designed in object oriented programming paradigm and implemented by using the C++ computer language. In order to facilitate the user to enter parameters, a user-friendly Graphic User Interface (GUI) is also implemented with the Tcl/Tk computer language as seen in Fig 3. After calculation, the incoming rays at the desired receiving point are illustrated in 3D graphics by using the Virtual Reality Modeling Language (VRML) as seen in Fig. 4. The program was compiled by using the GCC public domain C++ compiler and then run at a Sun Ultra-Sparc workstation. It can also work on a Intel Pentium processor running at 166 MHz and equipped with 32 MByte memory. Borland C++ is used to compile the program on PC.

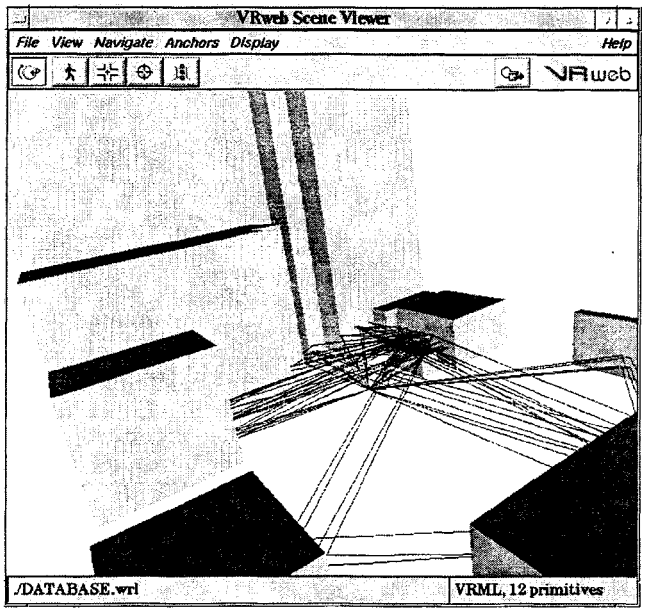

Fig. 4. 3D illustration of the received rays in VRML

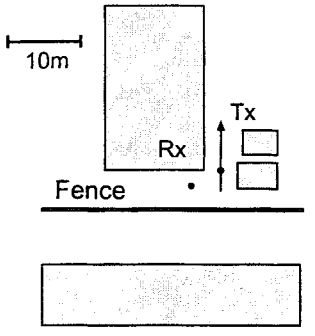

Fig. 5. Path-loss measurement environment

The accuracy of the code is verified by comparing the calculation result with measurement. The measuring environments are shown in Fig. 5 and Fig. 6. Both measurement sites are typical pico-cell cases with areas under 60 × 60 square meters. Since it is very difficult to verify the calculation accuracy of ray tracing in AOA, a good starting point is to compare ray-tracing results with measurement in pico-cell environments. The TIT measurement environment is rather simple and the YRP measurement environment is quite complex with mixed heights of buildings and a nearby hill. A metal pillar and doors are indicated by a square black box and thin black boxes. The heights of a car, buildings and antennas are also shown in the figure. The electrical parameters [24] used for the calculation of ray-tracing in all environments are listed in Table I.

The other simulation parameters are listed in Table II.

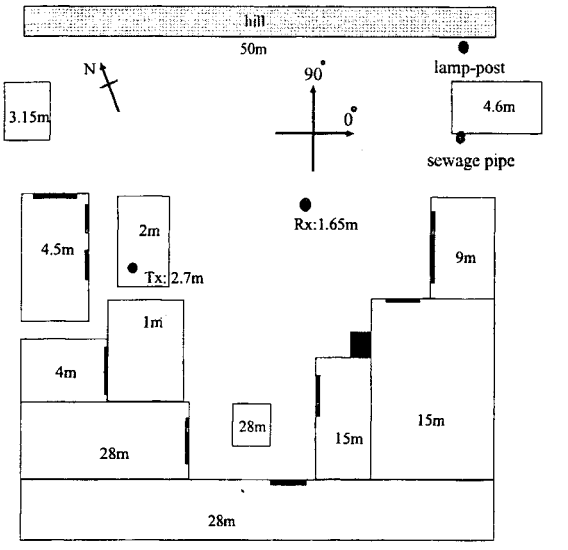

Fig. 6. Delay-profile measurement environment

TABLE I
ELECTRICAL PARAMETERS USED IN RAY-TRACING

	ϵ_r	σ [S/m]
building wall	5.5	0.023
ground plane	15.0	0.005
metal	-	∞
hill	3.5	0.01

By increasing the order of reflections and diffractions in these environments, the results did not change considerably. The measurements of path loss, delay profile, and AOA were carried out and compared with the ray-tracing results.

A. Path Loss

During the measurement, the transmitter moved from the line-of-sight (LOS) area to the non-LOS (NLOS) area while the receiver was put in a fixed position. The transmitter antenna was connected to a signal generator and 1.28 GHz CW signal of 10 dBm transmitted. A

TABLE II
SIMULATION PARAMETERS USED IN RAY-TRACING

	TIT	YRP
Carrier frequency [Hz]	1.28 G	8.45 G
Tx height [m]	1.45	2.7
Rx height [m]	1.45	1.65
Reflection no.	4	6
Diffraction no.	1	1
Antenna	V-polarized 0.5λ dipole	

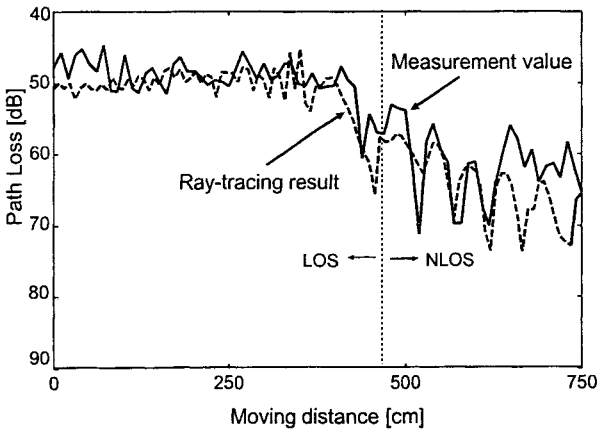

Fig. 7. Comparison of fast-fading variation of signal level between ray tracing and measurement

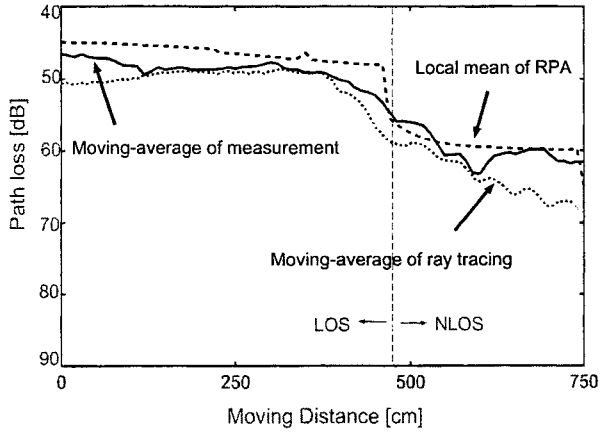

Fig. 8. Comparison of mean signal level between ray tracing and measurement

spectrum analyzer measured the received signal level. The whole moving range was 7.5 m and the transmitter moved at a step of 10 cm, which was nearly equal to 0.5λ of the CW signal.

Figure 7 shows the measured fast-fading pattern of signal level with the calculated ray-tracing result. The level deviation of the fast-fading signal can be observed at around 15 dB in the NLOS region. Figure 8 shows a local mean calculated over 1-meter range with the moving-average method for comparison. The local mean predicted from the RPA is also shown there. The improvement of accuracy by using the RPA can be seen in the NLOS region. That is becasue the result is more sensitive to phase-errors in the NLOS region. The underestimated result in the NLOS due to phase-errors can be improved by using local mean predicted from the RPA. Meanwhile, with the RPA, a 90% confidence interval is calculated as seen in Fig. 9. Almost all of the measurement data fell into this confidence interval. That proves that the RPA can predict the fluctuation range of the fast-fading signal.

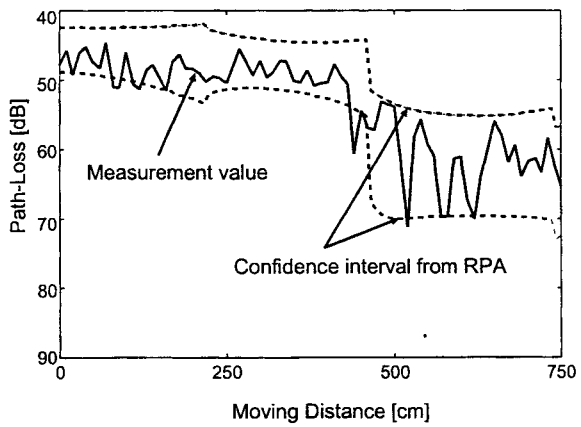

Fig. 9. Comparison of fading-fluctuation range between ray tracing and measurement

B. Delay Profile

The delay profile measurement is carried out in another pico-cellular environment as shown in Fig. 5. A delay profile measurement system utilizing pseudo noise (PN) code [25] is used here. A 8.45 GHz spread-spectrum signal with the rate of 50 Mchips/s was transmitted. The whole dynamic range is above 60 dB (2047 chips of PN length) and the whole bandwidth of this system is 100 MHz. The receiving antenna is moved at 8×8 grid points with a 0.4λ separation distance between grids. Since the scattering effects of a small hill near the receiving point can not be neglected, it is modeled as a tall rectangular obstacle. The effects of metal doors and pillars are also modeled in the ray-tracing process.

The delay profiles corresponding to 5%, 50% and 95% cumulative probabilities are extracted from all 64 measured delay profiles. Alternatively, the delay profiles corresponding to 5%, 50% and 95% cumulative probabilities derived from the random phase approach are then compared with measurement results. Figure 10 shows a high level of agreement between the median delay profiles of ray tracing and measurement. Especially, there is an almost 100% overlap of the peaks of direct wave, second arrival waves, third arrival waves in the graph. The over-estimation of ray tracing is observed at around 260 ns. This may be caused by inaccurate approximation of electrical parameters because the signal level is still strong enough after the ray traveled 78 meters. Figure 11 shows that the fluctuation range of measured delay profiles in this small area (about $4\lambda \times 4\lambda$) are almost totally confined within the 90% confidence

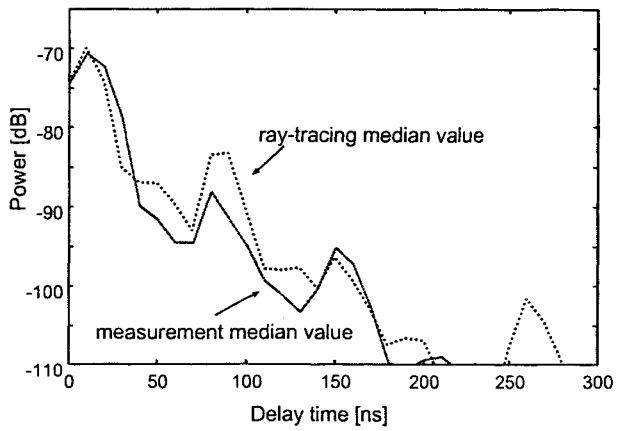

Fig. 10. Comparison of median delay profile between ray tracing and measurement

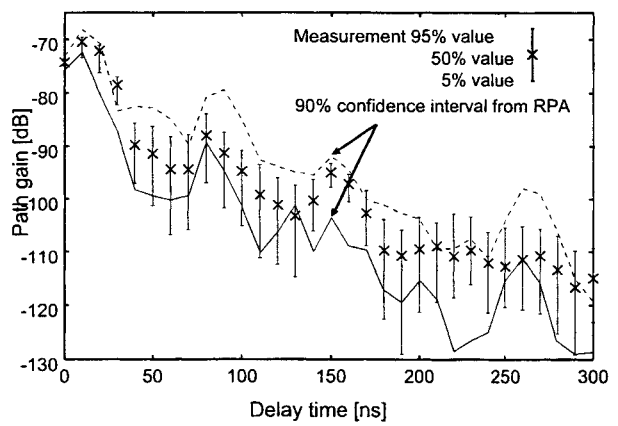

Fig. 11. Comparison of fluctuated delay profiles between ray tracing and measurement

interval calculated by the RPA. It proves that the RPA can predict an accurate short-term fluctuation range of delay profiles. In other words, the effects of inaccurate antenna positions (4λ in this case) can be also addressed.

C. Azimuth-Delay Profile

In this measurement, the measurement setup is the same as that described in the section III-B. To obtain a synthetic aperture, the receiving antenna is moved at 8×8 grid points with a 0.4λ separation distance of grids. A 8×8 2-dimensional array antenna system is therefore simulated. An azimuth-delay power profile (beamforming pattern) of this antenna system is calculated and compared with the corresponding ray-tracing result. The ray-tracing result is first transformed into the band-limited response in delay domain and then convolved with the antenna pattern to generate the beamforming pattern.

These azimuth-delay profiles are plotted in contour

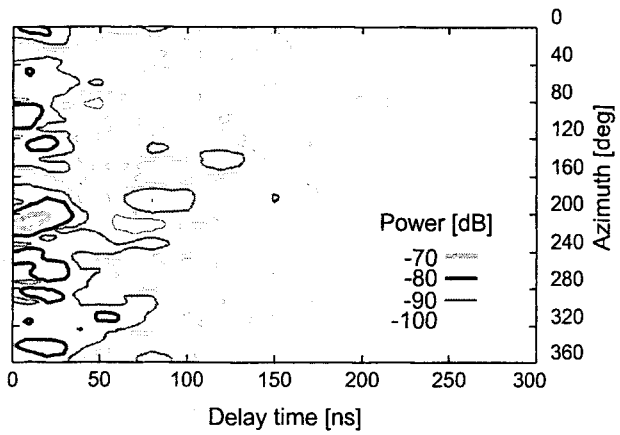

Fig. 12. Contour plot of the measured azimuth-delay profile

figures. Figure 12 shows the ray-tracing result. Figure 13 plots the measurement data. From these two graphs, a good agreement can be observed at direct waves (at around 200 degrees) and back-reflection waves (at 340 degrees). At these directions, the first, the second and the third arrival waves (for 200 degrees only) are all separated around 70 ns. Some angle deviations of the second and third arrival waves are also observed. These phenomena are all accurately predicted by ray tracing. However, the arrival waves between 40 degrees to 120 degrees are not predicted by ray tracing. Among these directions, there is almost an open space, because the hill is quite far away. Since they almost arrived at the same delay time as the direct waves, they can be understood as the local scattered waves by the nearby equipments.

Overall, the authors' ray-tracing tool showed a high level of accuracy and was fully verified with regard to the path loss, the delay profiles and the angle of arrival.

IV. Conclusion

This paper described a random-phase-assisted ray-tracing code, which is designed for predicting spatio-temporal channel parameters. The main purpose of this code is to provide an accurate prediction tool for deterministic wireless channel modeling. The RPA is applied in ray-tracing to give statistically correct results in the calculation of path loss and delay profiles. It was also found that the RPA could predict an accurate fading-fluctuation range of signal level and delay profiles. These advantages can not be achieved with the conventional ray-tracing codes. In addition to those, the authors also verified the prediction accuracy of the ray-tracing method with respect to angles. The further verification of this code in micro-cellular environments has been continued [26] and will be submitted as an-

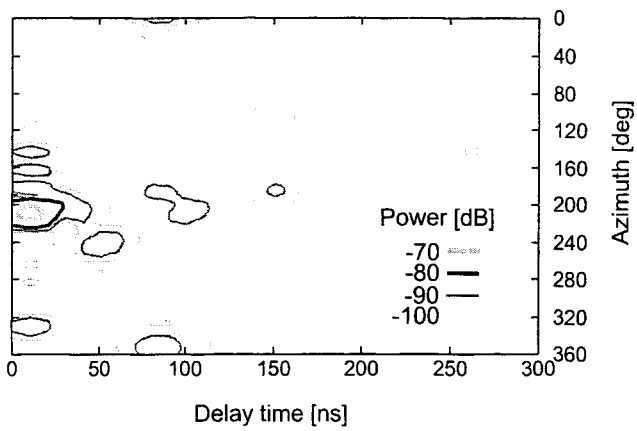

Fig. 13. Contour plot of the predicted azimuth-delay profile from ray tracing

other paper. The authors are continuing their efforts to launch a full-functional ray-tracing code both for channel modeling and network planning.

V. Acknowledgments

The authors would also like to thank K. Takiishi, J. Fu, N. Abe, N. Sakai, and K. Sakaguchi of Tokyo Institute of Technology, H. Masui, H. Shimizu, M. Ishii and K. Sakawa of YRP Key Tech Labs for their help in this work. This work is partly supported by the Scientific Grant in Aid from Japanese Society of Promotion of Science.

References

[1] V. Erceg, S. J. Fortune, J. Ling, A. J. Rustako, Jr., and R. A. Valenzuela, "Comparisons of a computer-based propagation prediction tool with experimental data collected in urban microcellular environments," *IEEE J. Selected Areas Commun.*, vol. 15, no. 4, pp. 677–684, May 1997.

[2] R. P. Torres, L. Valle, M. Domingo, S. Loredo and M. C. Diez, "CINDOOR: An engineering tool for planning and design of wireless systems in enclosed spaces," *IEEE Ant. & Prop. Mag.*, vol. 41, no. 4, pp. 11–22, Aug. 1999.

[3] Cátedra, M., J. Pérez, F. Saez de Adana, and O. Gutierrez, "Efficient ray-tracing techniques for three-dimensional analyses of propagation in mobile communications: application to picocell and microcell scenarios," *IEEE Ant. & Prop. Mag.*, vol. 40, no. 2, pp. 15–27, April 1998.

[4] T. Kurner, D. J. Cichon, and W. Wiesbeck, "Evaluation and verification of the VHF/UHF propagation channel based on a 3-D-Wave propagation model," *IEEE Trans. Ant. & Prop.*, vol. 44, no. 3, pp. 393–404, Mar. 1996.

[5] S. Y. Seidel, and T. S. Rappaport, "Site-specific propagation prediction for wireless in-building personal communication system design," *IEEE Trans. Veh. Tech.*, vol. 43, no. 4, pp. 879–891, Nov. 1994.

[6] G. Athanasiadou, A. Nix, J. McGeehan, "Comparison of predictions from a ray tracing microcellular model with narrowband measurements," at 47th IEEE Vehicular Technology Conference, pp. 800–804, Phoenix, May 1997.

[7] G. Durgin, N. Patwari, T.S., Rappaport, "An advanced 3D ray launching method for wireless propagation prediction," at 47th IEEE Vehicular Technology Conference, pp. 785–789, Phoenix, May 1997.

[8] K. Rizk, J. Wagen, and F. Gardiol, "Two-dimensional ray-tracing modeling for propagation prediction in microcellular environments," *IEEE Trans. Veh. Tech.*, vol. 46, no. 2, pp. 508–517, May 1997.

[9] A. G. Kanatas, I. D. Kountouris, G. B. Kostaras, and P. Constantinou, "A UTD propagation model in urban microcellular environments," *IEEE Trans. Veh. Tech.*, vol. 46, no. 1, pp. 185–193, 1997.

[10] S. Takahashi, Y. Yamada and K. Ogura, "Propagation-loss prediction using ray tracing with a random-phase technique," *IEICE Trans. Fundamentals*, vol. E81-A, no. 7, pp. 855–859, Jul. 1998.

[11] H. Zhu, J. Takada, and K. Araki, "The implementation of a 3D ray-tracing method for the spatio-temporal channel modeling," in the 433th URSI-F Japanese Committee meeting, April 1999.

[12] H. Zhu, J. Takada, and K. Araki, "Ray-tracing-based spatio-temporal channel modeling for multimedia mobile access communication systems (MMAC)," Int. Symp. on Personal, Indoor and Mobile Radio Comm. (PIMRC'99), pp. 116–120, Osaka, Sept. 1999.

[13] J. B. Keller, Geometric theory of diffraction, *J. Opt. Soc. Amer., 52,* pp. 116–130, 1962.

[14] J. D. Foley, A. van Dam, S. K. Feiner, J. F. Hughes, *Computer Graphics Principles and Practice*, pp. 660–663, Addison–Wesley, New York, 1997.

[15] C. Balanis, *Advanced Engineering Electromagnetics*, John Wiley & Sons, NewYork, 1989.

[16] O. Landron, M. J. Feuerstein and T. S. Rappaport, "A comparison of theoretical and empirical reflection coefficients for typical exterior wall surfaces in a mobile radio environment," *IEEE Trans. Ant. & Prop.*, vol. 44, no. 3, pp. 341–351, March 1996.

[17] R. J. Luebbers, "Finite conductivity uniform GTD versus knife edge diffraction in prediction of propagation path loss," *IEEE Trans. Ant. & Prop.*, vol. AP-32, no. 1, pp. 70–76, Jan. 1984

[18] A. Hammoudeh, M. Sánchez, and E. Grindrod, "Experimental analysis of propagation at 62 GHz in suburban mobile radio microcells," *IEEE Trans. Veh. Tech.*, vol. 48, no. 2, pp. 576–587, Mar. 1999.

[19] J. E. Hansen, *Spherical Near-Field Antenna Measurements*, pp. 312-342, IEE, London, 1988.

[20] V. Erceg, A. J. Rustako, Jr., and R. S. Roman, "Diffraction around corners and its effects on the microcell coverage area in urban and suburban environments at 900 MHz, 2 GHz, and 6 GHz," *IEEE Trans. Veh. Tech.*, vol. 43, no. 3, pp. 762–766, Aug. 1994.

[21] R. Barakat, "First-order statistics of combined random sinusoidal waves with applications to laser speckle patterns," *Optica Acta*, no. 11, pp. 903–921, 1974.

[22] J. K. Jao, and M. Elbaum, "First-order statistics of a non-Rayleigh fading signal and its detection," *Proc. IEEE*, no. 7, pp. 781–789, 1978.

[23] H. Zhu, J. Takada, K. Araki, H. Masui, M. Ishii, K. Sakawa, H. Shimizu, and T. Kobayashi, "Ray-tracing modeling and experimental verification of the spatio-temporal channel characteristics in a pico-cellular environment," *IEICE Tech. Rep.*, SST-62, pp. 75–82, Feb. 2000.

[24] CCIR Rec. 527-2, Electrical characteristics of the surface of the Earth, *Recommendations and Reports of the CCIR*, Vol. V, ITU, Geneva, 1991.

[25] H. Masui, K. Takahashi, S. Takahashi, K. Kage and T. Kobayashi, "Delay profile measurement system for microwave broadband transmission and analysis of delay characteristics in an urban environment," *IEICE Trans. Electron.*, no. 7, pp. 1287–1292, 1999.

[26] H. Zhu, J. Fu, J. Takada, K. Araki, H. Masui, M. Ishii, K. Sakawa, H. Shimizu, and T. Kobayashi, "An investigation of the spatio-temporal channel model in a suburban micro-

cellular environment," *IEICE Tech. Rep.*, SST-63, pp. 83-92, Feb. 2000.